The dehydrogenation of ammonia–borane catalysed by dicarbonylruthenacyclic(II) complexes†‡

Cédric Boulho and Jean-Pierre Djukic*

Received 31st March 2010, Accepted 26th June 2010
DOI: 10.1039/c0dt00241k

The reactivity of ruthenacyclic compounds towards ammonia–borane's dehydrogenation was investigated by considering both hydrolytic and anhydrous conditions. The study shows that the highly soluble μ-chlorido dicarbonylruthenium(II) dimeric complex derived from 4-*tert*-butyl,2-(*p*-tolyl)pyridine promotes, with an activation energy E_a of 22.8 kcal mol^{-1}, the complete hydrolytic dehydrogenation of NH_3BH_3 within minutes at *ca.* 40 °C. The release of 3 eq. of H_2 entails the formation of boric acid derivatives and the partly reversible *protonolysis* of the catalyst, which produces free 2-arylpyridine ligand and a series of isomers of "$Ru(CO)_2(H)(Cl)$". Under anhydrous conditions, hydrogen gas release was found to be slower and the dehydrogenation of NH_3BH_3 results in the formation of conventional amino–borane derivatives with concomitant *protonolysis* of the catalyst and release of isomers of "$Ru(CO)_2(H)(Cl)$". The mechanism of the *protonolysis* of the ruthenacycle was investigated with state-of-the-art DFT-D methods. It was found to proceed by the concerted direct attack of the catalyst by NH_3BH_3 leading either to the formation of a coordinatively unsaturated "$Ru(CO)_2(H)(Cl)$" species. The key role of "$Ru(CO)_2(H)(Cl)$" species in the dehydrogenation of ammonia–borane was established by trapping and quenching experiments and inferred from a comparison of the catalytic activity of a series of dicarbonylruthenium(II) complexes.

Introduction

Cycloruthenated aromatic ligands possess a large array of applications in homogenous catalysis and particularly in atom transfer processes, which are highly relevant to the design of rational and selective methods that meet one of the central green chemistry criteria, *i.e.* "atom economy". Among those processes hydrogen transfer holds a very important position.[1] Our recent effort in this field focused on revisiting the chemistry of chloridodicarbonyl ruthenacycles[2,3] long known for their robustness and, until recently, also known for an alleged relative chemical inertness. On this latter aspect recent investigations brought new elements of information on the possible domain of applications of this class of ruthenacycles in homogenous catalysis.[4,5] Stereoselective dimerisation of terminal alkynes into enynes[6] and hydrogenation of other disubstituted alkynes[7] offered particularly promising features. These studies also revealed the central role played by hydrido-ruthenium species especially in the stereospecific hydrogenation of diphenyl acetylene into *Z*-stilbene by metal-promoted hydrogen transfer from secondary alcohols.[7]

The recent upsurge[8] of interest for the metal-promoted production of molecular hydrogen by dehydrogenation[9] of ammonia–boranes[10–14] has led us to evaluate the propensity of ruthenacyclic compounds to act as catalysts. Our main concern being focused on the actual fate of the metallacycle and on identifying the most likely nature of the catalytic active species. The present paper discloses our main conclusions on the activity of an array of dicarbonylruthenacyclic complexes (Fig. 1), which were used as potential catalysts for the dehydrogenation of NH_3BH_3,[8] the nature of the catalytically active species and the limitations of the hereafter described system.

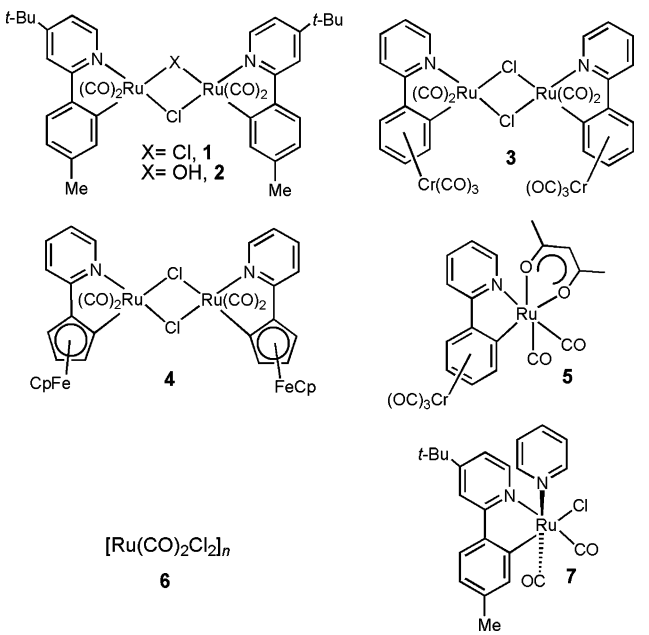

Fig. 1 Ruthenium(II) dicarbonyls considered in this study.

Institut de Chimie UMR 7177 CNRS, 4 rue Blaise Pascal, 67070, Strasbourg Cedex, France. E-mail: djukic@unistra.fr; Tel: 33368851 523

† In memory of *Pascal Le Floch*.

‡ Electronic supplementary information (ESI) available: (1) extensive crystallographic information for compound **7**, (2) extensive analytical data for **7** and other analytical evidence, and (3) cartesian coordinates of all intermediates and transitions states mentioned in this study with their energy and vibrational frequencies. CCDC reference number 771514 (**7**). For ESI and crystallographic data in CIF or other electronic format see DOI: 10.1039/c0dt00241k

Experimental

General

All experiments were carried out under a dry argon atmosphere using the standard Schlenk technique. Anhydrous THF was distilled from purple solutions of Na/benzophenone under argon. All other solvents were distilled over sodium or CaH_2 under argon. Deuterated solvents were dried over sodium or CaH_2 and purified by trap-to-trap techniques, degassed by freeze–pump–thaw cycles and stored under argon. ^{1}H, ^{13}C, ^{31}P and ^{11}B NMR spectra were obtained on Bruker DPX 300, 400 or Avance 500 spectrometers. Chemical shifts were referenced against solvent peaks or external references such as $BF_3{\cdot}Et_2O$ or H_3PO_4. Compounds **1–5**[2,3,7] were recently reported, and compound **6** was synthesized following Hiraki's procedure.[15] Standard experiments were carried out at room temperature (20 ± 1 °C). Deuterated ammonia–boranes were synthesized according to published procedures.[16]

Catalytic hydrogen release

Catalytic hydrogen release experiments were carried out in a special glass vessel consisting of a 10 mL flask soldered with a narrow section glass pipe to a U-shaped 20 mL volumetric burette (0.1 mL precision). The glass burette was filled with a low density silicon oil chosen so as to minimize the volume correction associated with the pressure exerted by the column of oil. The volume of released H_2 gas, assimilated here to a perfect gas, was read directly from the burette and corrected accordingly. The produced amount of molecular hydrogen was used to calculate c_r the hypothetical *equivalent residual molar concentration* in NH_3BH_3, *i.e.* $c_r = c_0[1 - (n_h/3n_0)]$, where n_h is the number of moles of H_2 produced and c_0 and n_0 are respectively the initial concentration and number of moles of NH_3BH_3.

Optimal procedure for the hydrolysis of ammonia–borane at room temperature

Ammonia–borane (8.4 mg, 0.27 mmol) and catalyst (0.04 mmol relative to Ru) were mixed and freshly distilled THF (2 mL) was added *via* a syringe. Upon equilibration of the inner vessel's pressure, water (100 μL, 5.55 mmol) was added *via* a micro-syringe to initiate the production of H_2. The reactions progress was monitored by measuring gas evolution volumetrically. During the reaction, a white inorganic solid precipitated. The solvent was removed under reduced pressure and the white residue was washed with water, acetone and then dried before performing solid state magic angle spinning ^{11}B NMR. Elem. anal. found: B, 18.86; H, 4.66; N, 7.53.

Competing hydrogen transfer reactions

Ammonia–borane (8.4 mg, 0.27 mmol), catalyst **1** (18.4 mg, 0.02 mmol), diphenyl acetylene (142 mg, 0.80 mmol) and 1,3,5-tri(*tert*-butyl)benzene (0.037 mmol) were dissolved in 2 mL of freshly distilled THF. Water (100 μL, 5.55 mmol) was added with a micro-syringe to initiate the reaction. Gas evolution was measured volumetrically. When hydrogen gas stopped evolving, the resulting solution was evaporated under reduced pressure. The overall yield in stilbenes was determined by ^{1}H NMR spectroscopy to 26% with a 5 : 1 ratio of *Z* and *E*-stilbene respectively. The same procedure was applied in the presence of indanone as the hydrogen atom acceptor (108 mg, 0.82 mmol) and led to 42% yield in 1-indanol. Adjusting the molar ratio of ammonia–borane *vs.* 1-indanone to 1 : 1 afforded 94% yield in 1-indanol.

Protonolysis of 1 with d_3 and d_6 ammonia–boranes under anhydrous conditions

Deuterated ammonia–borane (ND_3BH_3, NH_3BD_3 and ND_3BD_3) (0.65–2.65 mmol) and complex **1** (0.24–0.36 mmol) were introduced in a Schlenk tube in a glovebox and dissolved in 10 mL of dry THF. After 7 h of reaction a sample of the reaction mixture was transferred to an NMR sample tube and analysed by ^{2}H NMR analysis to check for the presence of dissolved HD or D_2 gas. After one night the resulting brown solution was passed through a short silica gel column (eluent CH_2Cl_2/acetone 20 : 1), the filtrate was stripped of solvent under reduced pressure and the residue containing free ligand **9** further submitted to two consecutive chromatographic separations. The ligand was recovered with a reasonable purity upon chromatographic separation on preparative thick silica gel layer plates using as eluent a 20 : 1 and a 20 : 0.5 mixture of CH_2Cl_2 and acetone. ^{1}H NMR and ^{2}H NMR spectroscopic characterizations were carried out respectively in d_6-acetone and in a mixture of CH_2Cl_2 and C_6F_6 (lock signal on ^{19}F) with minor amounts of CD_2Cl_2 as reference.

Variable sub-ambient temperature NMR experiments

Complex **1** (4.0 mg, 0.005 mmol) and NH_3BH_3 (2.0 mg, 0.065 mmol) were introduced in an NMR sample tube and d_8-tetrahydrofuran was added. The tube was cooled to –60 °C, water (5 μL, 0.278 mmol) was added by a microsyringe and the tube was introduced in the NMR spectrometer's probe.

Reaction monitoring by NMR spectroscopy

Three separate stock solutions of reagents dissolved in d_8-tetrahydrofuran, namely complex **1** (c = 0.038 mM), NH_3BH_3 (c = 0.52 mM) or ND_3BH_3 (c = 0.52 mM) were prepared. 1,3,5-Tris(*tert*-butyl)benzene was chosen as the internal reference and was combined to the solution containing compound **1** (c = 0.025 mM). Catalyst solution (400 μL) was hence introduced in two separate NMR sample tubes, which were cooled down to –50 °C prior to the addition of the solution of ammonia–borane (150 μL) *via* a syringe. NMR sample tubes were subsequently introduced carefully in the NMR spectrometer's probe.

Catalytic H_2 release monitored by fuel-cell's response to partial H_2 pressure variation

Two stock solutions containing respectively compound **1** (c = 17 mM) and NH_3BH_3 (c = 265 mM) in dry THF were prepared in separate Schlenk tubes. A volume of tetrahydrofuran (1.05 mL) was injected in the clean and dry reaction vessel through which a steady stream 11.5 mL min^{-1} of argon, used here as a carried gas, was flowed in the hydrogen compartment of a LightFC-1U fuel-cell (http://www.h2economy.com) *via* a 95 cm long 1.5 mm inner diameter coiled Teflon hose. Standard settings implied the concomitant steady flow of air in the fuel-cell's oxygen

compartment at a value of 12.5 mL min^{-1}. The fuel-cell's electrodes were preliminary plugged to an ADC 42 Picotechnologies™ analogic-logic signal converter connected to a computer in order to acquire the variations of potential over time with a sampling frequency of 10 Hz. In a typical experiment, 50 s after the start of signal acquisition a volume of the stock solution of catalyst was injected in the reaction vessel, followed at t = 150 s by a volume of the stock solution of ammonia-borane and at t = 250 s by a volume of pure distilled water (0.05 mL, 2.8 mmol).

Synthesis of (*OC*-6-54)-biscarbonyl,chlorido,pyridine[4-(*tert*-butyl),2-(4-methylphenylene,κC_2)pyridine,κ*N*] ruthenium(II), compound 7

In a Schlenk tube, pyridine (32 µL, 0.40 mmol) was added to a THF solution (15 mL) of **1** (157 mg, 0.188 mmol). The solution was stirred for 24 h at room temperature and the solvent was evaporated under reduced pressure. The yellow residue was recrystallized by adding pentane in a concentrated solution in dichloromethane (98 mg, 52% yield). Suitable crystals for X-ray diffraction (Fig. 2) were obtained by slow diffusion of *n*-pentane in a dichloromethane solution of the complex. Elem. anal. calc. for $C_{23}H_{23}N_2O_2ClRu{\cdot}1/8\ CH_2Cl_2$: C, 54.83; H, 4.63; N, 5.53. Found: C, 55.09; H, 4.59; N, 5.64. IR (ATR) ν_{max}/cm^{-1} 2027 (CO), 1955 (CO). δ_H ($CDCl_3$; 298 K) 9.41 (d, 1H, $^3J_{HH}$ = 6.1 Hz, H_{Phpy}), 8.53 (d, 2 H, $^3J_{HH}$ = 5.0 Hz, H_{py}), 7.73 (d, 1H, $^4J_{HH}$ = 2.0 Hz, H_{Phpy}), 7.67 (s, 1H, H_{Phpy}), 7.59 (t, 1H, $^3J_{HH}$ = 7.6 Hz, H_{py}), 7.59 (d, 1H, $^3J_{HH}$ = 8.0 Hz, H_{Phpy}), 7.20 (dd, 1H, $^3J_{HH}$ = 6.1 Hz, $^4J_{HH}$ = 2.0 Hz, H_{Phpy}), 7.10 (dd, 2H, $^3J_{HH}$ = 7.4-6.6 Hz, H_{py}), 6.90 (d, 1H, $^3J_{HH}$ = 8.0 Hz, H_{Phpy}), 2.36 (s, 3H, H_{Phpy}), 1.33 (s, 9H, H_{Phpy}). δ_C ($CDCl_3$; 298 K) 200.6, 196.9 (CO), 169.0 (C_{Phpy}), 164.1 (C_{Phpy}), 163.6 (C_{Phpy}), 152.1 (C_{py}), 149.2 (C_{Phpy}), 141.6 (C_{Phpy}), 141.0 (C_{Phpy}; C_{Phpy}), 138.3 (C_{py}), 125.1 (C_{py}), 125.0 (C_{Phpy}), 124.6 (C_{Phpy}), 119.9 (C_{Phpy}), 115.8 (C_{Phpy}), 35.7 (C_{Phpy}), 30.8 (C_{Phpy}), 22.1 (C_{Phpy}).

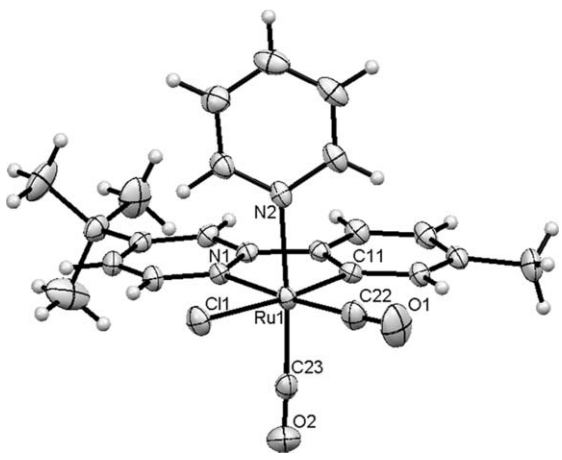

Fig. 2 CSD Mercury ellipsoid view of the structure of complex **7**. This view represents half of the asymmetric cell content, which contains another identical molecule of the same compound. Ellipsoids are drawn at the 30% probability level. Selected interatomic distances (in Å): Ru1–Cl1 2.4737(6), Ru1–C11 2.055(2), Ru1–C22 1.878(2), Ru1–C23 1.870(2), Ru1–N1 2.1295(16), Ru1–N2 2.1758(18), C22–O1 2.1758(18), C23–O2 1.126(3). Selected interatomic angles (°): N1–Ru1–C11 79.15(7), N1–Ru1–Cl1 93.90(5), N2–Ru1–C23 176.02(8).

Structural X-ray diffraction analysis of 7§

Reflections were collected with a Bruker Apex II-CCD diffractometer using Mo-Kα graphite-monochromated radiation (λ = 0.71073 Å). The structure of **7** was solved by direct methods using the programme SHELXS-97.[17] The refinement and all further calculations were carried out using SHELXL-97.[18] The H-atoms were included in calculated positions and treated as riding atoms using SHELXL default parameters. The non-H atoms were refined anisotropically, using weighted full-matrix least-squares on F_2.

Theoretical investigations

The optimized geometries of singlet ground states and transition states as well as electronic structures were obtained by using the methods of the density functional theory (DFT) and completed with the computation of the vibrational modes. The dispersion-corrected *Becke*[19]-*Perdew*[20,21] GGA functional, *i.e.* BP86-D, implemented in the *Amsterdam Density Functional*[22,23] package was used throughout our investigation (*ADF2008.01 version*[24]). The semi-empirical treatment of dispersion includes long-range electron correlations by adding atom-pair wise dispersion corrections of the form C_6R^{-6} to the standard functionals, where R are interatomic distances and C_6 are the dispersion coefficients. Default recommended settings for the empirical dispersion correction were used with a factor of 1.050, van der Waals radii were scaled by 1.10.[25] In these calculations scalar relativistic effects were treated within the *Zeroth Order Regular Approximation*[26,27] (ZORA). As a consequence, in all cases and for all atoms *ad hoc* all-electron triple-ζ basis sets augmented with the adequate single-ζ polarization function, *i.e.* TZP, were used.[28] For substrates, adducts and intermediates geometry optimizations by energy gradient minimization, as well as transition state searches were carried out in all cases without symmetry constraint with an integration accuracy comprised between 4.5 and 6, an energy gradient convergence criterion of 10^{-3} au and with tight SCF convergence criteria. Vibrational modes were computed within the harmonic oscillator approximation either analytically or by numerical differentiation. The latter method was used systematically to compute both the vibrational modes and the thermodynamic data (internal energy and entropy) when solvation was accounted for with the COSMO procedure. With gas phase structures the analytical method was favored instead. Enthalpies were calculated in kcal mol^{-1} by the summation of the total bonding energy, fragments energy, internal energy (zero point vibrational energy-inclusive) and the product of the perfect gas constant R with absolute standard temperature in Kelvin (298.15 K). Isotopic effects were computed with Klamt's solvation COSMO procedure on, considering the Born–Oppenheimer principle by substituting were applicable protium atoms for deuterium in the considered optimized geometries and by re-computing vibrational modes and concomitantly the associated statistical thermodynamic data by the two-point numerical differentiation method. Klamt's COSMO[29] treatment of solvation was applied using the procedure

§ $C_{23}H_{23}ClN_2O_2Ru$, M = 495.95, monoclinic, a = 17.6291(5) Å, b = 11.5208(3) Å, c = 24.1776(6) Å, β = 115.955(2)°, V = 4415.2(2) $Å^3$, T = 173(2) K, space group $P2_1/c$, Z = 8, 33 642 reflections measured, 11 736 unique (R_{int} = 0.020) which were used in all calculations. The final w$R(F_2)$ was 0.065 (all data).

implemented within the ADF package with Klamt's adjustments of the van der Waals radii of atoms. Counterpoise correction for basis set superposition error (BSSE) was neglected due to the exclusive use of triple-ζ basis sets.[30] Representations of molecular structures and orbitals were drawn using *ADFview* v08.

Results and discussion

There are several accepted modes of dehydrogenation of NH_3BH_3[8,9,31,32] and as far as metal-promoted processes are concerned two types of such modes can be considered in a first instance. The first one entails the release of H_2 by the formal oxidation of NH_3BH_3 into NH_2BH_2, the following steps leading to the complete extrusion of H_2 and the formation of polymers and oligomers generally formulated as $(N_xB_xH_y)_n$,[10,12,33–44] the recycling of which has become a matter of active investigation.[45–48] The second process is the "hydrolytic" dehydrogenation[11,49–52] of NH_3BH_3 into molecular hydrogen and borates of various possible formulations, a process that can be metal-promoted and which is generally effective not only in the presence of water but also in other protic solvents.[13,53–60] Of particular interest are those hydrolytic conditions proposed by Jagirdar *et al.*[54] and Xu *et al.*,[11] in which non-noble metal salts are used as precursors of metallic nanoparticles that act as catalysts. Distinguishing between these two possible modes, *i.e.* hydrolytic *vs.* anhydrous, was the first objective of this study as shown in the following. For the sake of commodity compound **1** was chosen as a lead for all investigations that were carried out.

Evidence for catalyst-dependent hydrolytic pathway

The hydrolytic decomposition of NH_3BH_3 was tested by using complex **1** as a prototypical catalyst precursor, and by varying the concentration of H_2O dissolved in anhydrous and distilled tetrahydrofuran at room temperature (20 ± 1 °C) (Fig. 3). Fig. 3 displays the rate of release of equivalents of H_2 *vs.* time at various amounts of water. It is evident from this curve that adding as little as 1 eq. of water triggers the decomposition of NH_3BH_3 and the release of about 2 eq. of H_2 in less than 1 h. In the absence of water, one can notice only low residual production of hydrogen.

Improved hydrogen production is obtained with 2 eq. of water, which allows the release of about 2.5 eq. of H_2 in about 1 h. A feature that was not fully understood is the apparent inhibition of hydrogen production upon increase of the amount of water added from 2 to 4 eq., which tends to limit the amount of releasable H_2 to *ca.* 2.5 eq. Also, one can notice in Fig. 3(a) a slight induction period of about 5 to 10 min before the effective start of H_2 production. This induction period during which H_2 production is negligible vanishes above 4 eq. of added water. The inhibition process is held back apparently with 20 eq. of water, which allows the release of 3 eq. of H_2 within about 2 h (Fig. 3(b)). Moreover, under identical conditions, the use of D_2O inhibits the production of dihydrogen, of which the content in deuterium was not sought at this stage. The production of 1 eq. of hydrogen gas takes less than 20 min and more than 30 min when H_2O and D_2O are used respectively.

Dependence towards catalyst

In the following investigation, conditions ensuring a fast and efficient production of H_2 with a rather moderate amount of water were chosen, that is by carrying out the reaction in THF in the presence of 20 eq. of water relative to NH_3BH_3 with compound **1** as the catalyst. A relative first order in catalyst at a steady concentration in NH_3BH_3 in the presence of 20 eq. of water was also verified by the linear relationship existing between the apparent rate of release of H_2 and catalyst concentration (Fig. 4), demonstrating *de facto* the key role of compound **1** in the hydrolytic release of H_2 from NH_3BH_3. Under identical conditions at 20 °C the apparent first order in NH_3BH_3 at steady concentration in **1** could be readily established (Fig. 5).

Under optimal hydrolytic conditions, the relation of the rate of release of H_2 to temperature was readily established. The Arrhenius plot depicted in Fig. 6 is related to a value of 22.8 kcal mol^{-1} for the activation energy E_a, a value that compares well with those obtained with other catalytic systems designed for the hydrolytic decomposition of ammonia–borane.[55,61] A temperature of +40 °C corresponds to an optimum for a swift release of 3 molar eq. of H_2.

Relatively accurate proof for the formation of H_2 as well as valuable information on the response time of the catalytic system was obtained by acquiring the variation of electric potential at the connectors of a H_2/air fuel-cell. Analytical proof for the formation of other gases such as B_2H_6 or NH_3 was not sought. This system

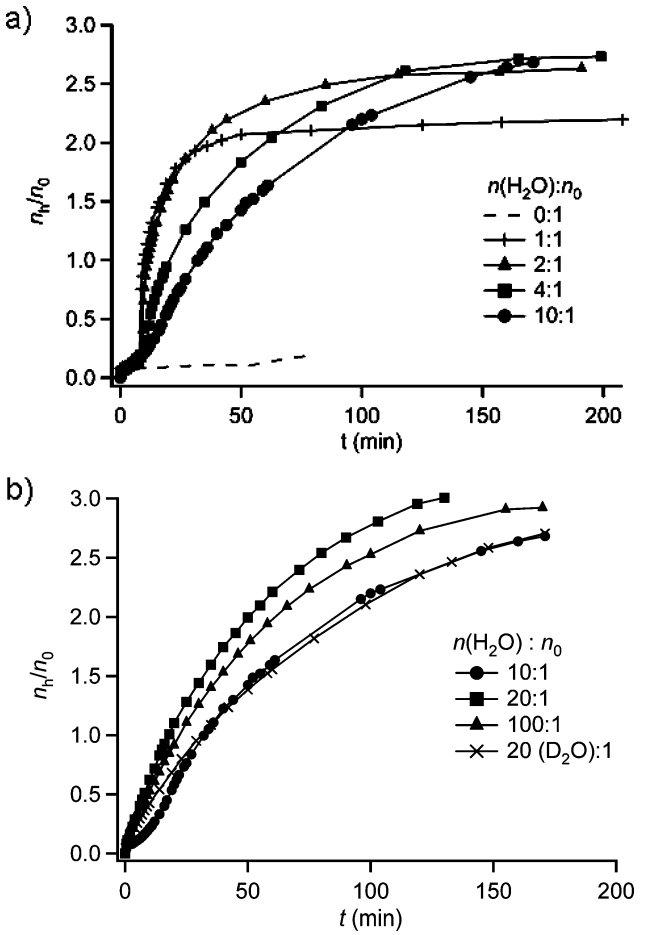

Fig. 3 Molar equivalent of evolved dihydrogen *vs.* time at various concentrations in H_2O at 20 ± 1 °C: (a) in the 0 to 10 molar eq. excess of water relative to NH_3BH_3; (b) in the 10 to 100 eq. excess of water range relative to NH_3BH_3.

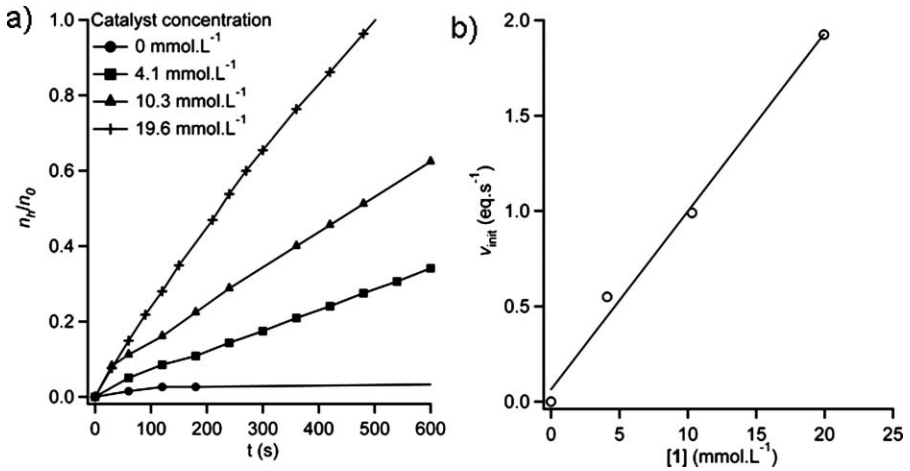

Fig. 4 (a) Molar equivalent of evolved dihydrogen *vs*. time at various concentrations of **1** (*i.e.* 8.2, 20.6, 29.9 and 39.3 mM relative to Ru); (b) plot of the initial hydrogen release rate v_{init} *vs*. the concentration in catalyst **1**.

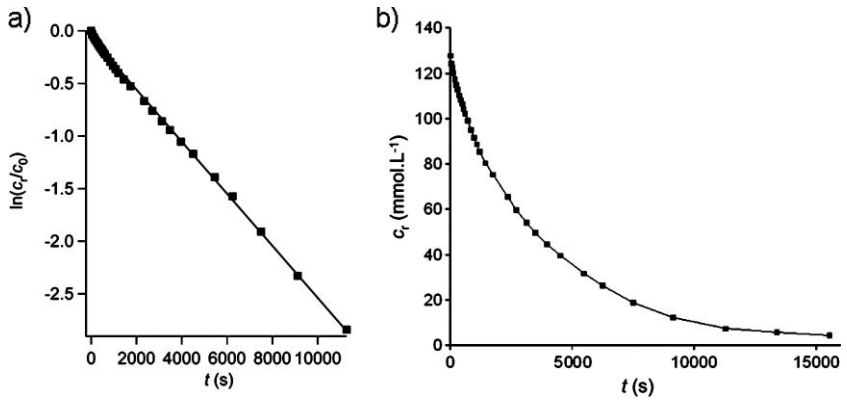

Fig. 5 (a) evolution of residual ammonia–borane concentration *vs.* time and (b) typical first order in ammonia–borane's concentration logarithmic profile *vs.* time (s).

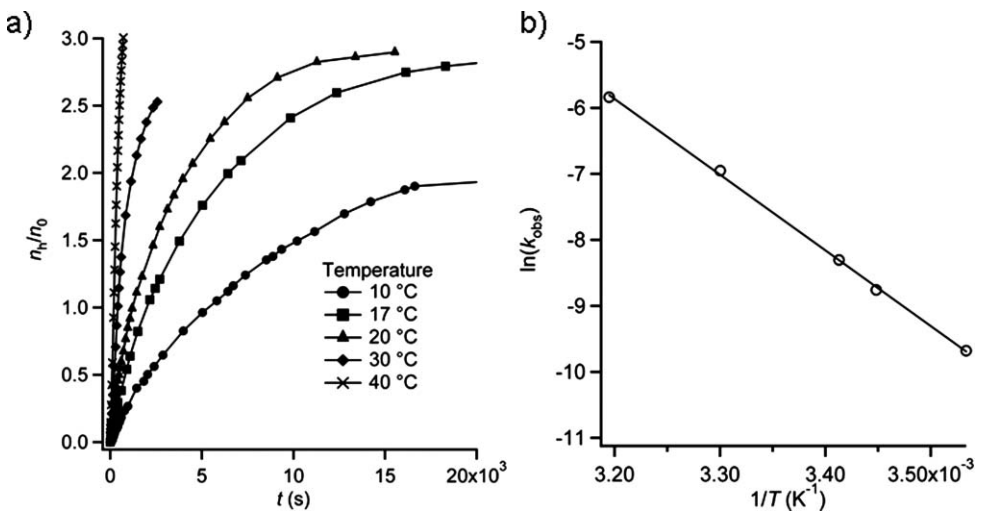

Fig. 6 Temperature-dependence of the rate of release of H_2 with identical concentrations of catalyst **1** and water: (a) plot of molar eq. of released H_2 *vs*. time; (b) Arrhenius plot of the logarithm of observed H_2-release rate constant *vs*. reciprocal absolute temperature.

was used here as a qualitative analytical tool allowing the measure of the instantaneous partial H_2 pressure released by the catalytic pot. Connected *via* a narrow and long Teflon hose to the hydrogen compartment of the fuel cell, the reaction vessel was permanently flushed with a steady flow of dry argon gas. Fig. 7, which displays a diagram of the experimental set up, shows several plots of the difference of potential U (mV) at the fuel-cell *vs.* time (s). Notably the production of H_2 is sensible in all cases from the moment NH_3BH_3 is added to the solution containing the catalyst. In the absence of water the rate of production of H_2 is low (lower partial pressure). The peculiar peak feature observed at t = 500 s might be related to an inherent feature of fuel-cells, *i.e.* the so-called "concentration polarisation" effect. In the presence of water in the reaction vessel, the production of H_2 is much faster and clearly depends upon catalyst concentration.

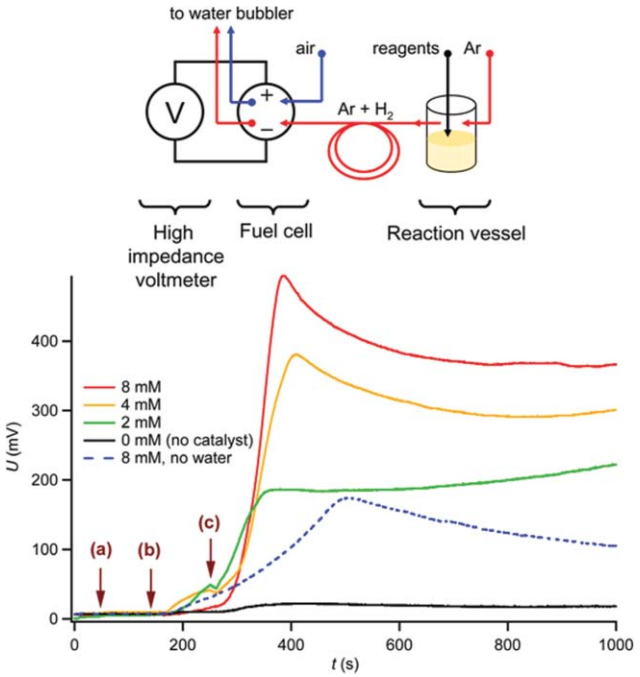

Fig. 7 The release of H_2 was monitored by capturing the variation of potential at the plugs of a single stack fuel-cell. The peak feature occurring at $t \sim 400$ s is assigned to the fuel-cell's inherent so-called *concentration–polarisation* effect. (a) Injection of a volume of the catalyst mother solution. (b) Injection of a volume of NH_3BH_3 mother solution. (c) Injection of water.

The fate of the reaction components

In the presence of water

A particular feature of this catalysed hydrolytic decomposition of NH_3BH_3 is the significant change of colour from light yellow to dark brown and the formation of an insoluble precipitate that occurs in the course of the reaction.

The composition of the reaction medium was analysed by ^{11}B (referenced against BF_3–Et_2O) and ^1H NMR spectroscopies by staging the NH_3BH_3 degradation reaction in an NMR sample tube filled with d_8-THF and by monitoring the changes in the spectra as temperature was raised stepwise from –60 °C to +20 °C in the presence of water. Noteworthy, the composition of the reaction medium changes drastically upon warming from –60 °C to –10 °C (Fig. 8). Compound **1**, which exists as a mixture of μ-chlorido-bridged dimers provides in the ^1H NMR spectrum at room temperature about four groups of signals between δ 8.8 and 9.6 ppm arising from the phenylpyridyl ligands of about four different diastereomers. This feature was reproduced at –60 °C in the initial solution that already contained substantial amounts of dissolved NH_3BH_3. Warming this mixture to –10 °C resulted in a major simplification of this region of the ^1H NMR spectrum, which is symptomatic of the formation of a new mononuclear ruthenacyclic complex, *i.e.* adduct **8** that results from the coordination of NH_3BH_3 onto a mononuclear unit of **1**. The broad signals at δ 5.50 and 6.40 ppm account for a coordinated molecule of NH_3BH_3 subjected to fast exchange (Fig. 8) and are likely to be related to species **8**. It is worth noting, when ND_3BH_3 was used in another experiment, these two broad signals were not observed, thus suggesting that they relate to the H atoms borne by the nitrogen centre.

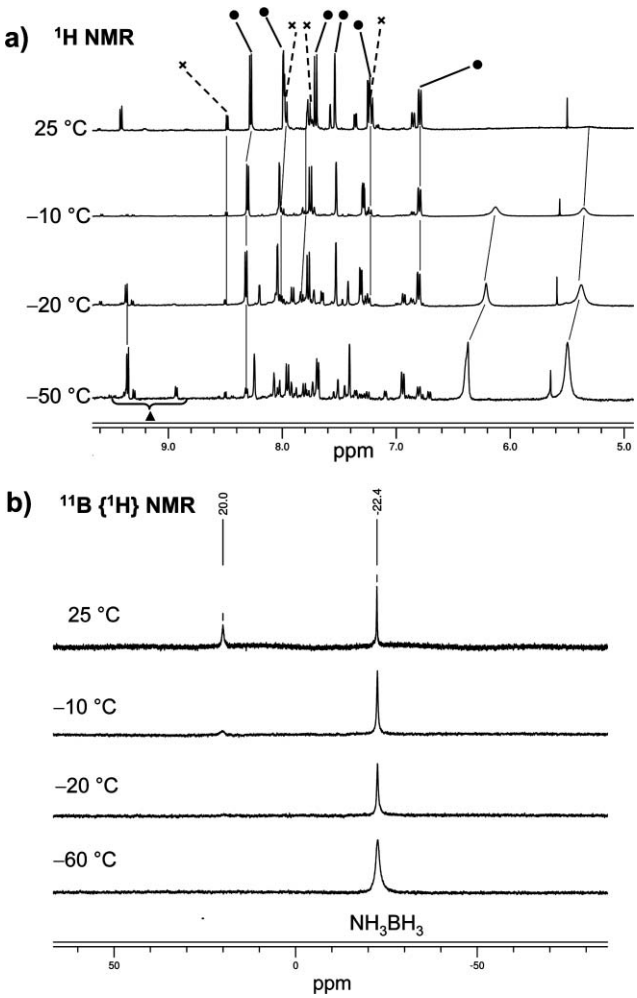

Fig. 8 (a) ^1H and (b) ^{11}B $\{^1H\}$ NMR spectra of a d_8-THF solution of a mixture of catalyst **1** (5×10^{-2} M), NH_3BH_3 (16×10^{-2} M) and H_2O (70×10^{-2} M) at various temperatures. (a) ▲, **1**; ●, **8**; ×, ligand **9**.

Once the reaction mixture was warmed to 25 °C, spectroscopic analysis indicated the reformation of substantial amounts of

complex **1** and the presence of species **8** and free ligand **9** (Scheme 1).

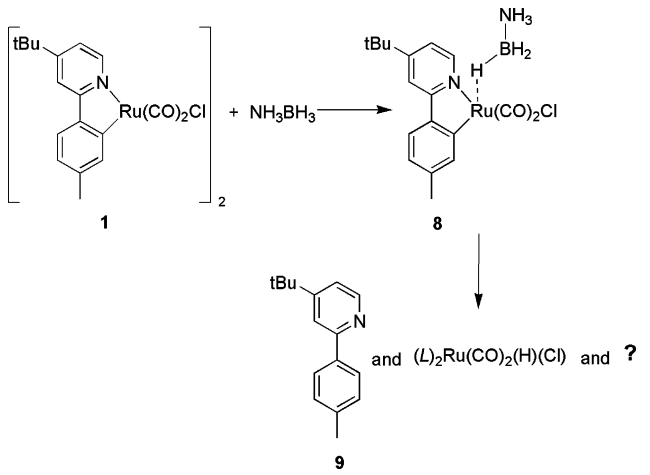

Scheme 1 Protonolysis of catalyst **1** by ammonia–borane.

The proton-decoupled ^{11}B NMR spectra (Fig. 8(b)) that were acquired from –60 up to –20 °C are not informative of the presence of any other boron-containing species but NH_3BH_3. This situation changes upon warming to room temperature. The ^{11}B signal appearing at *ca.* +20 ppm agrees well with recent reports made for the ^{11}B NMR spectra of boric acid derivatives in solution.[54,62,63]

A ^{11}B MAS NMR experiment was also carried out with the off-white precipitate that was collected upon complete release of 3 eq. of H_2; the resulting spectrum was found to be quite similar in chemical shift and in line shape to that of commercial boric acid. This microcrystalline solid was also submitted to elemental analysis. This analysis revealed a content in nitrogen of 7.58% mass, which suggests that mono ammonium tetraborate salt $(NH_4)HB_4O_7$ is one of the components of this insoluble solid material. This information also suggests that this solid precipitate, which is insoluble in conventional organic solvents, differs in nature from the species observed in solution and from which the low-field ^{11}B signal arises.

It is estimated that about 10 to 20% of compound **1** undergoes protonolysis under these conditions. The product of this de-chelation process was trapped by quenching the catalytic pot with an excess of PPh_3 and the resulting mixture was analyzed by ^1H NMR spectroscopy. The latter indicated the presence of major amounts of $(PPh_3)_2Ru(CO)_2(Cl)(H)$, of which spectral and analytical data were in accord with data found in the literature.[64,65] The origin of this species can only be related to the protonolysis of a derivative of **1** containing the $Ru(CO)_2(Cl)$ motive. The most reasonable chemical formulation of the released hydrido-ruthenium species is either that of a mononuclear solvate, *i.e.* $(thf)_2Ru(CO)_2(Cl)(H)$ or that of a polynuclear μ-hydrido and μ-chlorido bridged complex. Water does not seem to be directly responsible for the production of ligand **9** from **1**. Ruthenacycles such as **1** are insensitive to water unless placed in the presence of a mild base, which essentially promotes the formation of **2** (Fig. 1).

In anhydrous conditions

A reaction of compound **1** with a large excess of NH_3BH_3 in dry d_8-tetrahydrofuran as well as in dry d_6-benzene led to the release of significant amounts of metal-free ligand **9** as observed in the corresponding ^1H NMR spectra. In the experiment carried out in d_6-benzene, singlets typical for Ru–H species[7] were also noticed at high field, *i.e.* δ –8.48, –8.76, –9.76 ppm in a 2 : 2 : 1 ratio. In the experiment performed in dry d_8-tetrahydrofuran, two main singlets of identical intensities typical of hydrido-ruthenium species were observed at δ –8.98 and –9.31 ppm. It is worth noting here that the ^{11}B NMR spectra of the reaction mixture indicated explicitly, after 16 h of reaction, the presence of dehydrogenated derivatives of ammonia–borane, such as polyaminoboranes and the cyclic borazine (Fig. 9). According to both ^1H-decoupled and raw ^{11}B NMR spectra, borazine's and polyaminoborane typical signals were found respectively at δ +28.8 ppm and in the –4.5 to –16.0 ppm region.[32,33,40,66,67] Further proof for the intervention of hydrido-ruthenium species in the hydrolytic process of dehydrogenation of NH_3BH_3 was also sought by introducing amounts of an hydrogen acceptor, such as 1,2-diphenylethyne or 1-indanone, in the reaction medium (*cf.* ESI, Fig. S10†).[7] Quite expectedly the hydrogenation of indanone "consumes" about half of the amount of potentially available H_2-equivalent within 3 h in a reaction that produces 1-indanol in 42% yield. 1,2-Diphenylethyne is selectively hydrogenated into *Z* and *E*-stilbenes in 26% yield.

$$[Ru(CO)_2Cl_2]_n + LiEt_3BH + \mathbf{9} \xrightarrow{THF,\ room\ temp.} \mathbf{1} \text{ and } [(L)_2Ru(CO)_2(H)(Cl)]_n \text{ and } ? \quad (1)$$

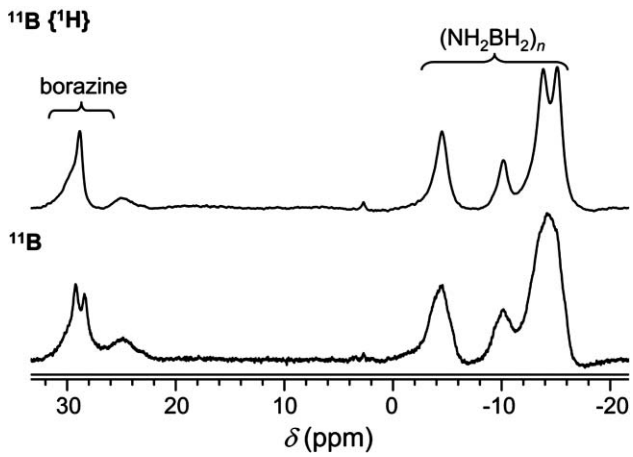

Fig. 9 ^{11}B $\{^1H\}$ and ^{11}B NMR spectra of the solution resulting from the reaction of NH_3BH_3 with **1** in anhydrous THF after 16 h of reaction.

At this stage, the partial reversibility of protonolysis of the metallacycle was qualitatively verified by undertaking the reaction of $[Ru(CO)_2Cl_2]_n$ with a mixture of $LiEt_3BH$ and ligand **9** in THF for one week (eqn (1)). This experiment led to the formation of a dark brown mixture containing, according to ^1H NMR analysis in $CDCl_3$, 36% mol of isomers of complex **1** and other species formulated as $[(L)_2Ru(CO)_2(Cl)(H)]_n$ (L = **9**) that displayed typical hydridic ^1H singlets at around δ –17.0 and –17.8 ppm.

Labeling experiments under anhydrous conditions

In this study, we also investigated the effect of isotopic labeling over the protonolysis process by resorting to deuterated ammonia–boranes. The use of dry solvents and reagents was found mandatory when using ND_3BH_3, for residual H_2O could readily deplete the content in deuterium by isotopic scrambling and, therefore, introduce a detrimental bias in the assessment of deuterium incorporation. Parallel experiments were carried out in an argon-filled dry-box using ND_3BH_3 and NH_3BD_3, which were prepared according to literature procedures and checked for purity in the solid-state by FT-IR using an ATR cell. Typical experiments were carried out in dry THF by reacting a large amount of complex **1** with labeled ammonia–borane for 24 h at room temperature. About 7 h after the beginning of both experiments, samples of each reaction mixture were withdrawn and analysed by proton-decoupled ^{2}H NMR spectroscopy in order to check for the presence of a labeled form of dissolved dihydrogen, *i.e.* HD or D_2. The spectrum corresponding to the experiment carried out with NH_3BD_3 clearly showed the presence of two singlets at δ 4.57 ppm and at 4.52 ppm corresponding respectively to HD and D_2. When ^{1}H-decoupling was lifted, the signal at 4.57 ppm turned into a doublet with a ^1J coupling constant of 42 Hz characteristic of HD.[68–70] Quite surprisingly, the ^{2}H NMR spectrum of the reaction medium containing ND_3BH_3 displayed only the signal assigned to HD and no signal for D_2.

A pure sample of **9** was extracted from the resulting mixture after *ca.* 16 h of reaction and was analysed by ^{1}H and ^{2}H NMR spectroscopy in order to evaluate the % of incorporated deuterium. The spectra confirmed that deuterium was exclusively incorporated at the tolyl's *ortho* position relative to the pyridyl substituent. In the experiments carried out with ND_3BH_3 and NH_3BD_3 the amount of incorporated deuterium was 22% and 78%, respectively, with respect to one out of two identical *ortho* position. It is worth noting that the use of perdeuterated ammonia–borane, *i.e.* ND_3BD_3, under identical conditions led to 110% deuterium incorporation, which conspicuously further supports the hypothesis of a reversible protonolysis.

Theoretical investigation of catalyst protonolysis

In recent reports dealing with metal-catalysed dehydrogenation of ammonia–borane the high potential of chelated complexes[43] such as $Ir(H)_2(POCOP)$[40] was praised, however, the exact fate of the catalyst and the possible co-existence in the catalytic pot of competing catalytically active species were not addressed. In the following, we focus on the unexpected protonolysis of the Ru (+II) dicarbonyl unit. The computational investigation was carried out using DFT (density functional theory) within the ADF framework.[22] In this study, we have chosen to apply a state-of-the-art DFT-D (dispersion-corrected DFT) approach, the systematic use of which has been recently advocated[71] for the achievement of reliable descriptions of situations (intermediates and transition states) whereby non-covalent interactions[72] play a central role. DFT-D computations in this study were carried out by means of the Becke-Perdew density functional empirically corrected for *dispersion*, *i.e.* BP86-D, which is an accepted[73] fair compromise between reliability and computational time effectiveness.[71] All calculations were also carried out within the relativistic Zeroth Order Regular Approximation (ZORA) with Slater-type all-electron triple ζ polarized basis sets (STO TZP) and without symmetry constraint. The study was performed considering the system in the gas phase and in tetrahydrofuran by applying Klamt's solvation model, *i.e.* COSMO. A simplified model of **1**, *i.e.* **S1** (Fig. 10), was considered. Its optimized ground-state structure displayed good agreement with available X-ray diffraction data of **1**.[7] For instance, the dispersion-sensitive Ru–Ru distance, that amounts to 3.782 Å in **1** amounts to 3.727 Å in **S1**, is well reproduced. The largest deviation of about 0.02 Å from experimental values is observed for the $C_{Ar\text{-}ipso}$–Ru distance, which amounts to 2.046(3) in **1** and 2.067 Å in model **S1**.

Our analysis of the reaction energy profile was conditioned by the observations made for the protonolysis of **1** by NH_3–BH_3 under anhydrous conditions. Experimental evidence suggests that two processes coexist, that are namely: (1) the protonolysis leading to free ligand **9** (here modeled as 2-phenylpyridine) and a new hydrido,chlorido,dicarbonylruthenium(II) species, and (2) a secondary reverse cyclometalation process. The protonolysis invoked here implies three events that may occur in successive steps *or* in a concerted manner. First, an ammonia–borane adduct with the ruthenium complex must form. Subsequently, a proton-trapping step, similar to that put forward by Fagnou *et al.*[43] and by Hall *et al.*[38,39] occurs with the transfer of an acidic hydrogen from the ammonia part of NH_3BH_3 to a nucleophilic centre at the catalyst. The hydride transfer step ensues from the hydridic borane part to the Lewis-acidic ruthenium centre.

In our computations (Fig. 10) we considered the preliminary step to be the formation of an adduct similar to **8** (of which two conformers **A1** and **A2** are considered here) consisting of a molecule of NH_3BH_3 axially coordinated through one of its hydridic boron-bound hydrogens to the Ru centre of a mononuclear unit formed upon splitting of dimer **S1**.

In the lowest potential energy conformer **A1**, the BH_3 part interacts through one of its hydridic hydrogens with the ruthenium centre (Ru–H(B) distance amounts to 1.820 Å) whereas the NH_3 fragment interacts with the chlorido ligand ((N)H $\cdots$ Cl distance amounts to 1.995 Å). This privileged conformation results from a highly favourable electrostatic situation as suggested by the Coulombic potential map drawn over an isosurface of the SCF density (*cf*. ESI‡).[74] The latter map shows large accumulation of charges at the chlorido ligand (as well as at carbonyl ligands terminal oxygen atoms *cf*. ESI‡) leading to optimal interaction between the bonded polarised ammonia–borane molecule, *i.e.* δ^+H–N(H)$_2$(H)$_2$B–Hδ^- and the δ^+Ru–Cl δ^- segment. This conformation might prefigure another ammonia–borane activation route, which is not addressed here.

The second conformer **A2** possesses the proper orientation for direct interaction with the carbon atom of metallacycle. However, for reasons related to unfavorable orbital and electrostatic interactions, the formal carbanionic component of chelate does not appear to be particularly prepared for optimal interaction with the acidic NH_3 fragment of NH_3BH_3. In this conformer the (B)H–Ru, $C_{Ar\text{-}ipso} \cdots$ H(N) and $C_{Ar\text{-}ipso}$–Ru distances amount to 1.823 Å, 2.276 Å and 2.072 Å respectively. Analysis of the Coulombic potential maps[74] did not reveal any significant accumulation of charges in the vicinity of arene's metallated position. Furthermore, the highest occupied molecular orbital (HOMO) indicated no

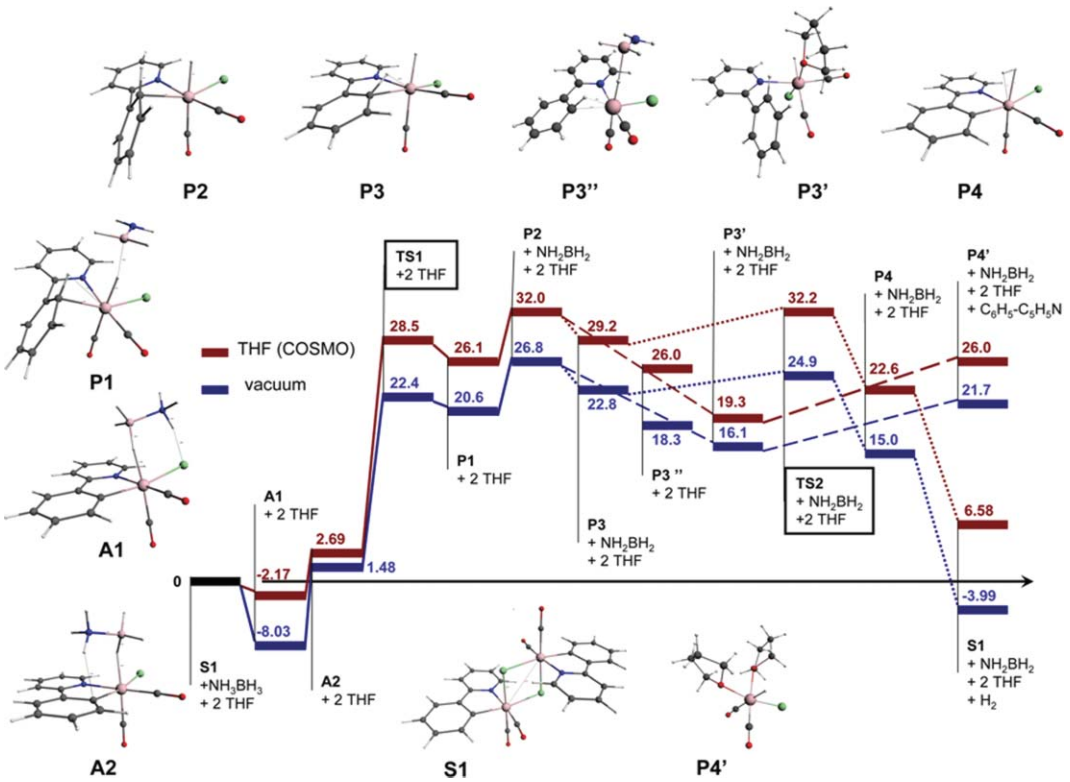

Fig. 10 Overall profile of the reaction of NH_3BH_3 with dimer **S1** and the associated gas-phase computed structures. Enthalpies (kcal mol^{-1}) were computed relative to the sum of enthalpies of the starting reaction components (*cf.* Scheme 2 for an explicit formulation of the mechanism). Levels in blue and in red correspond to DFT-D BP86-D/TZP(ZORA) calculations (ADF2008) carried out in the gas phase and by accounting for solvation by THF (COSMO procedure) respectively.

large orbital coefficient at this *ipso* position, which otherwise could have eased a bonding interaction with the acidic hydrogens of the NH_3 moiety. In fact, to induce the cleavage of the C–Ru bond, computation suggests that a significant activation barrier is necessary [at 298.15 K, $\Delta G^{\neq}_{\mathbf{A2}\text{-}\mathbf{TS1}}$ = 21.8 kcal mol^{-1} (vacuum), 23.8 kcal mol^{-1} (THF)], which implies a marked distortion of the metallacycle as depicted in transition state **TS1**, the structure of which suggests a concerted process (Fig. 11). This distortion of the ruthenacycle is essential for the effective "protonolysis" of the Ru–C_{Ar} bond. This late transition state contains a σ-type Ru–H–B interaction wherein the ruthenium-bound hydrogen atom exhibits a strong hydridic character. **TS1** leads to product complex **P1** which converts into **P2**. The relationship between **A2**, **TS1** and **P1** was verified by performing an internal reaction coordinate (IRC) search along the pathway defined by the first eigenvalue of the hessian matrix, which yielded the minimum energy reaction pathway accounted for therein.

It is worth noting that the use of the conventional BP86 functional, *i.e.* the density functional devoid of the specific semi-empirical treatment of dispersion, would not allow proper geometry convergence for **P1** and would lead to the disruption of the weak and mostly non-covalent interaction established between the polar NH_2BH_2 and the ruthenium-bound hydrido ligand in our calculations at the (ZORA) BP86-D/TZP level. This interaction of Coulombic and dispersive nature contributes significantly in lowering the enthalpy of the system by *ca.* 6 kcal mol^{-1}.

The process may subsequently take two different pathways. The first one that leads to **P3′** accounts for the protonolysis process and the formation of $(thf)_2Ru(CO)_2(H)(Cl)$, *i.e.* **P4′** (Fig. 10).

The second pathway accounts for the reverse cyclometalation process observed experimentally, which is possible through intermediates **P3″** and **P3**, *via* transition state **TS2** (Fig. 11), which leads to dihydrogen complex **P4** and eventually to dimer **S1** upon extrusion of H_2 and recombination (Fig. 10 and Scheme 2). Intermediates **P3″** and **P3** are similar in geometry to the rare cases of complexes whereby it has been established that the ruthenium centre is bonded to the chelating ligand *via* an agostic three center $C_{Ar} \cdots H \cdots Ru$ interaction.[75–77]

Similar stabilization was noticed for intermediate **P3″**, which lies 3–4 kcal mol^{-1} below dissociated **P3** + NH_2BH_2 as a result of a weak interaction between the Ru-bound hydrido ligand and NH_2BH_2. The possible role of the latter in a polarisation of coordinated H_2 in a transition state of formula [**TS2** $\cdots$ NH_2BH_2]$^{\neq}$, which could ease the reverse **P4**-to-**P3** process, was not investigated here although its mediacy is likely in light of the recent work published by Kawano *et al.*[14] Nonetheless, the relatively low forward and backward activation free energies for the **P3**–**TS2** and the **P4**–**TS2** steps give credit to a rather reversible protonolysis.

To account for the significant although incomplete incorporation of deuterium in metal-free ligand **9** (here modeled by 2-phenylpyridine), which is released by the protonolysis process either upon action of ND_3BH_3 (22% incorporation on one *ortho* site) or of NH_3BD_3 (78% incorporation on one *ortho* site) in

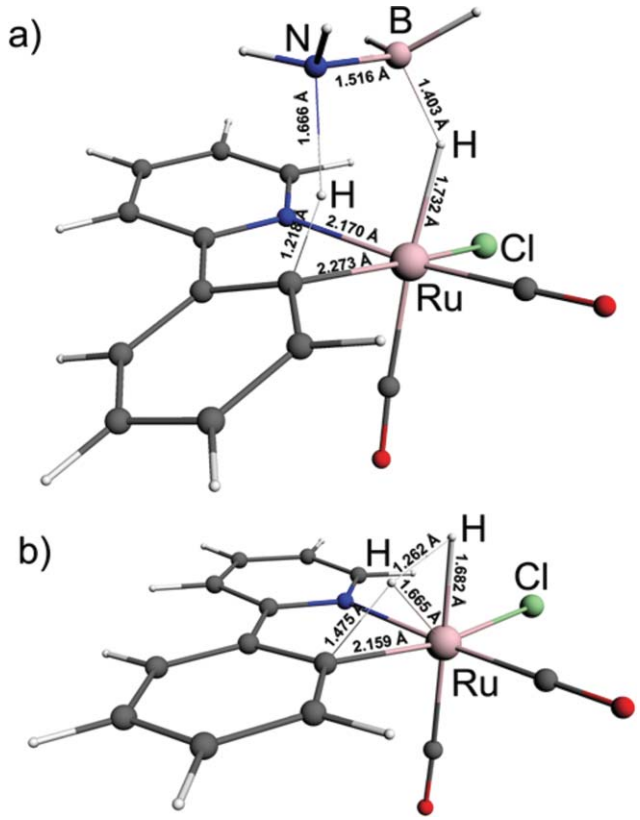

Fig. 11 Gas-phase transition state structures computed at the BP86-D/TZP (ZORA) level. (a) **TS1**: *i*507.5 cm^{-1} [THF(COSMO) *i*340.9 cm^{-1}]. (b) **TS2**: *i*970.7 cm^{-1} [THF(COSMO) *i*988.5 cm^{-1}].

anhydrous conditions, we evaluated the theoretical isotopic effects $(k_H/k_D)_f$ and $(k_H/k_D)_b$ associated with the activation barriers **P3**–**TS2** and **P4**–**TS2** respectively (Table 1) by considering the two positions the deuterium atom can possibly occupy (Scheme 3). Table 1 depicts a rather contrasted situation for the forward and backward paths; the latter being much less discriminating towards deuterium than the former. Nonetheless the rather high isotopic effects computed for both situations {D–H} and {H–D} in the **P3**–**TS2** direction could account for the incorporation of deuterium in released **9**. However, the fact that this incorporation is not 100% at one *ortho* position of **9** points to a more complex mechanistic reality: most of the hydrogen atoms incorporated into **9** upon protonolysis are provided by the BH_3 fragment. The higher deuterium incorporation noticed when using NH_3BD_3 can only be related to an effective H/D scrambling process operating at hydrogen intermediate **P4**. The hypothesis of such a scrambling is supported by the spectroscopic observation of dissolved D_2 in the reaction medium resulting from the reaction of **1** with NH_3BD_3 in anhydrous conditions. This behaviour has already been widely established for the reaction of other hydroboranes with transition metal complexes.[36,38,39,78–82]

Further evidence for the central role of a non-chelated $Ru(CO)_2$ species from a comparison of various catalysts

Fig. 12 displays the plot of the released equivalents of hydrogen *vs.* time for reactions carried out under identical conditions with the catalysts depicted in Fig. 1. From this plot it is tempting to infer

Table 1 Computed barriers of activation (in kcal mol^{-1}) for the forward **P3**–**TS2** and backward **P4**–**TS2** paths and the associated isotopic effects in two situations wherein one deuterium atom alternatively replaces a protium atom at ligand **9** and at the ruthenium centre in transition state **TS2** and the related intermediates (Scheme 3). Solvation by THF was accounted for using the COSMO method

	$\Delta G^{\neq}_{P3-TS2}$	$(k_H/k_D)_f$	$\Delta G^{\neq}_{P4-TS2}$	$(k_H/k_D)_b$
{H–H}	2.9		10.1	
{D–H}[a]	4.0	6.8	10.5	1.9
{H–D}[b]	3.5	3.1	10.4	0.6

[a] Protium borne by the ruthenium centre; **TS2**, *i*748.1 cm^{-1}. [b] Deuterium borne by the ruthenium centre; **TS2**, *i*953.8 cm^{-1}.

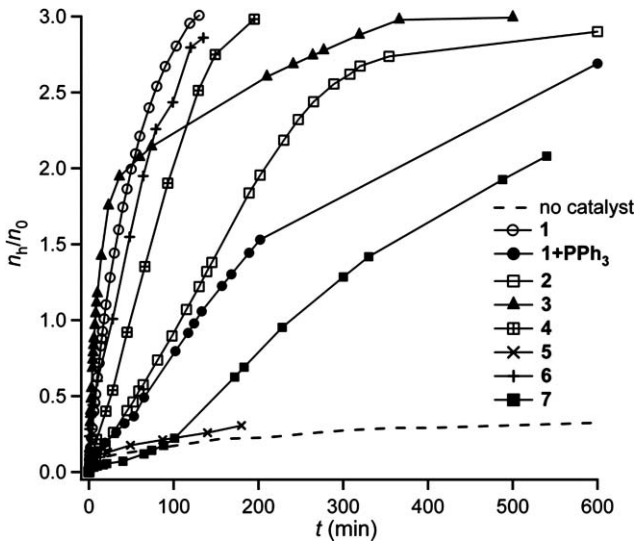

Fig. 12 Plot of the relative number of molar equivalents of released H_2 gas *vs.* time for different catalysts under identical hydrolytic conditions.

that the quasi-identical kinetic profiles determined for compounds **1** and **3**, **4** and **6** relate to a common active catalytic species resulting from the release of the $Ru(CO)_2Cl$ motive. This can be rationalized by the existence of readily accessible coordination sites at the ruthenium center of these μ-chlorido-bridged dimers, which allows interaction with NH_3BH_3 and further protonolysis of the catalyst, leading to the release of the "$Ru(CO)_2(Cl)(H)$" moiety from compounds **1**, **3** and **4**, or to the rapid formation of this hydrido-ruthenium species from **6**. From a mechanistic point of view, the study by Kawano *et al.*[14] of the dehydrogenative capability of electron-unsaturated chromium carbonyls provides a reasonable framework for understanding the mode of action of "$Ru(CO)_2(Cl)(H)$".

Slightly attenuated catalytic behaviour was obtained with compound **2** and with a mixture of **1** and triphenylphosphine. In the case of **2**, we speculate that the slight inhibition of the H_2 release as compared to **1** might probably express the enhanced stability of the μ-chlorido, μ-hydroxo bridging situation.[7] The hydroxo ligand does not have any promoting effect as internal base neither.[7] Addition of PPh_3 to **1** seemingly leads to the disruption of the μ-chlorido-bridged dimer and to the formation of a less labile 18 electron monoruthenium species. The curve related to the use of compound **7** depicts an even lower activity than for the **1** + PPh_3 mixture, which confirms that the use of fully "electron

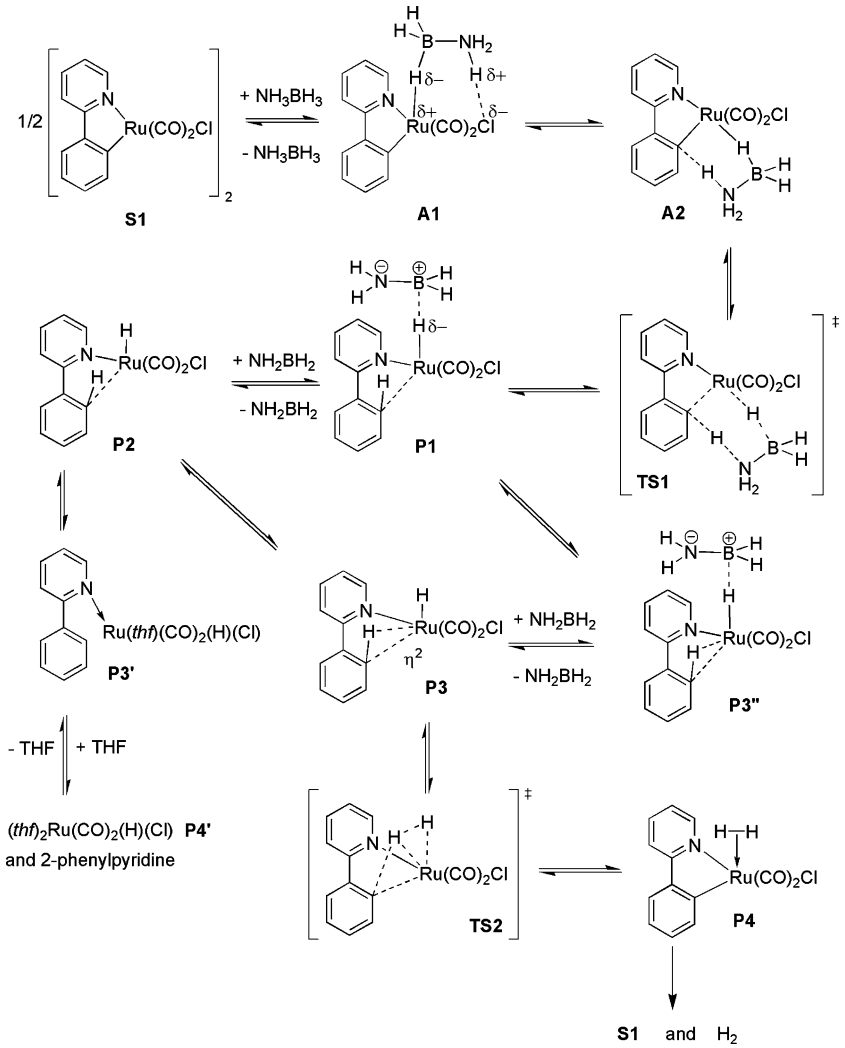

Scheme 2 Simplified protonolysis reaction mechanism.

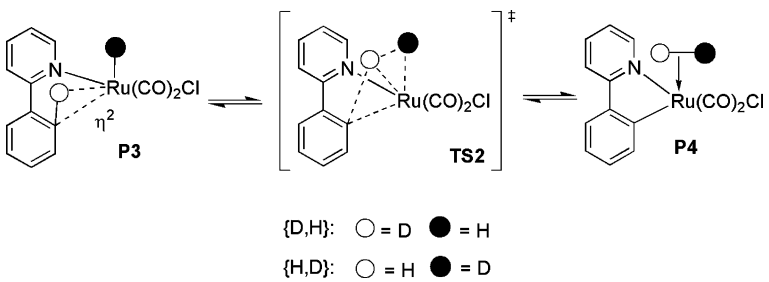

Scheme 3 The reversible dehydrogenative cyclometallation of intermediate **P3**.

saturated Ru complexes" is highly detrimental to catalytic activity. In line with the latter conclusion, the acetylacetonate ruthenium complex **5**, which as such represents an extreme case of unlabile bischelate complex, displays no major catalytic activity.

Conclusions

In this article we have disclosed a new property of ruthenacyclic complexes, *i.e.* their ability to promote the de-hydrogenation of ammonia–borane under anhydrous and hydrous conditions. From the point of view of hydrogen gas release, optimized hydrolytic conditions (40 °C) allow the complete release of 3 eq. of H_2 from 1 eq. of NH_3BH_3 within minutes and the formation of boric acid derivatives. The actual mechanism of formation of the latter inorganic products remains unknown. Experiments carried out under anhydrous conditions indicate that ammonia–borane reacts in a concerted manner with the ruthenacyclic catalyst to release a new coordinatively unsaturated hydrido, chlorido, dicarbonylruthenium species. Protonolysis of the Ru–C bond of **1** is a common feature under hydrous and anhydrous conditions;

it appears to be moderately reversible and to be a key step in formation of the central catalytic species "$Ru(CO)_2(Cl)(H)$" responsible for the dehydrogenation of ammonia–borane. Labeling experiments with d_3-ammonia–boranes, which also revealed the complexity of the system, point to a rather conventional behaviour of borane's derivatives towards transition metal centres, *i.e.* their capability to undergo hydrogen atom scrambling quite readily. The reason for the low hydrogen release rate under anhydrous conditions can be related either to the lack of sufficient reactivity of the "$Ru(CO)_2(Cl)(H)$" species or to a major interaction of NH_2BH_2 with unreacted NH_3BH_3 in the course of the dehydrogenation process, in a way similar to that proposed by Baker *et al.* recently.[33] The diversity of amino–borane products obtained under anhydrous dehydrogenation conditions compares well with that obtained with other catalytic systems. The rather higher rate of hydrogen gas release under hydrolytic conditions could be linked to the ruthenium promoted decomposition of highly reactive water adducts formed with NH_2BH_2. The exact role of water remains to be fully elucidated though.

Acknowledgements

The authors thank Prof. Dr S. Grimme (University of Münster, Germany) for fruitful discussions on issues related to DFT-D computations. The Centre National de la Recherche Scientifique, the Ministry of Education and Research and the National Research Agency (ANR-06-JCJC 0086-01) are gratefully acknowledged for their financial support. Dr Lydia Brelot (University of Strasbourg) is thanked for the structural X-ray diffraction characterization of compound **7**.

Notes and references

1 J.-P. Djukic, J.-B. Sortais, L. Barloy and M. Pfeffer, *Eur. J. Inorg. Chem.*, 2009, 817–853.
2 A. Hijazi, J. P. Djukic, M. Pfeffer, L. Ricard, N. Kyritsakas-Gruber, J. Raya, P. Bertani and A. de Cian, *Inorg. Chem.*, 2006, **45**, 4589–4591.
3 A. Hijazi, J. P. Djukic, L. Allouche, A. de Cian, M. Pfeffer, X.-F. Le Goff and L. Ricard, *Organometallics*, 2007, **26**, 4180–4196.
4 S. M. Islam and C. R. Saha, *J. Mol. Catal. A: Chem.*, 2004, **212**, 131–140.
5 D. K. Mukherjee, B. K. Palit and C. R. Saha, *J. Mol. Catal.*, 1994, **88**, 57–70.
6 A. Hijazi, K. Parkhomenko, J.-P. Djukic, A. Chemmi and M. Pfeffer, *Adv. Synth. Catal.*, 2008, **350**, 1493–1496.
7 J.-P. Djukic, K. Parkhomenko, A. Hijazi, A. Chemmi, L. Allouche, L. Brelot, M. Pfeffer, L. Ricard and Xavier-Frédéric Le Goff, *Dalton Trans.*, 2009, 2695–2711.
8 F. H. Stephens, V. Pons and R. T. Baker, *Dalton Trans.*, 2007, 2613–2626.
9 B. Peng and J. Chen, *Energy Environ. Sci.*, 2008, **1**, 479–483.
10 A. Staubitz, A. Presa-Soto and I. Manners, *Angew. Chem., Int. Ed.*, 2008, **47**, 6212–6215.
11 Q. Xu and M. Chandra, *J. Power Sources*, 2006, **163**, 364–370.
12 M. E. Sloan, T. J. Clark and I. Manners, *Inorg. Chem.*, 2009, **48**, 2429–2435.
13 Y. Li, L. Xie, Y. Li, J. Zheng and X. Li, *Chem.–Eur. J.*, 2009, **15**, 8951–8954.
14 Y. Kawano, M. Uruichi, M. Shimoi, S. Taki, T. Kawaguchi, T. Kakizawa and H. Ogino, *J. Am. Chem. Soc.*, 2009, **131**, 14946–14957.
15 K. Hiraki, Y. Obayashi and Y. Oki, *Bull. Chem. Soc. Jpn.*, 1979, **52**, 1372–1376.
16 M. Hu, J. van Paaschen and R. Geanangel, *J. Inorg. Nucl. Chem.*, 1977, **39**, 2147–2150.
17 G. M. Sheldrick, *Acta Crystallogr., Sect. A: Found. Crystallogr.*, 1990, **46**, 467–473.
18 M. Sheldrick, Universität Göttingen, Göttingen, Germany, Editon edn, 1998.
19 A. D. Becke, *Phys. Rev. A: At., Mol., Opt. Phys.*, 1988, **38**, 3098–3100.
20 J. P. Perdew, *Phys. Rev. B: Condens. Matter*, 1986, **34**, 7406.
21 J. P. Perdew, *Phys. Rev. B: Condens. Matter*, 1986, **33**, 8822–8824.
22 G. te Velde, F. M. Bickelhaupt, S. J. A. van Gisbergen, C. Fonseca-Guerra, E. J. Baerends, J. G. Snijders and T. Ziegler, *J. Comput. Chem.*, 2001, **22**, 931–967.
23 in *Amsterdam Density Functional*, ed. SCM, Department of Theoretical Chemistry, Vrije Universiteit Amsterdam, The Netherlands, edn, 2003.
24 E. J. Baerends, J. Autschbach, D. Bashford, A. Bérces, F. M. Bickelhaupt, C. Bo, P. M. Boerrigter, L. Cavallo, D. P. Chong, L. Deng, R. M. Dickson, D. E. Ellis, M. van Faassen, L. Fan, T. H. Fischer, C. Fonseca Guerra, A. Ghysels, A. Giammona, S. J. A. van Gisbergen, A. W. Götz, J. A. Groeneveld, O. V. Gritsenko, M. Grüning, F. E. Harris, P. van den Hoek, C. R. Jacob, H. Jacobsen, L. Jensen, G. van Kessel, F. Kootstra, M. V. Krykunov, E. van Lenthe, D. A. McCormack, A. Michalak, M. Mitoraj, J. Neugebauer, V. P. Nicu, L. Noodleman, V. P. Osinga, S. Patchkovskii, P. H. T. Philipsen, D. Post, C. C. Pye, W. Ravenek, J. I. Rodríguez, P. Ros, P. R. T. Schipper, G. Schreckenbach, M. Seth, J. G. Snijders, M. Solà, M. Swart, D. Swerhone, G. te Velde, P. Vernooijs, L. Versluis, L. Visscher, O. Visser, F. Wang, T. A. Wesolowski, E. M. van Wezenbeek, G. Wiesenekker, S. K. Wolff, T. K. Woo, A. L. Yakovlev and T. Ziegler, in *Amsterdam Density Functional*, ed. SCM, Department of Theoretical Chemistry, Vrije Universiteit Amsterdam, The Netherlands, Editon edn, 2008.
25 S. Grimme, *J. Comput. Chem.*, 2006, **27**, 1787–1799.
26 E. van Lenthe, A. E. Ehlers and E. J. Baerends, *J. Chem. Phys.*, 1999, **110**, 8943–8953.
27 E. van Lenthe, E. J. Baerends and J. G. Snijders, *J. Chem. Phys.*, 1993, **99**, 4597–4610.
28 E. van Lenthe and E. J. Baerends, *J. Comput. Chem.*, 2003, **24**, 1142–1156.
29 A. Klamt and G. Schüürmann, *J. Chem. Soc. Perkin Trans.*, 1993, 799–805.
30 A. Rosa, A. W. Ehlers, E. J. Baerends, J. G. Snijders and G. te Velde, *J. Phys. Chem.*, 1996, **100**, 5690–5696.
31 A. Staubitz, M. Besora, J. N. Harvey and I. Manners, *Inorg. Chem.*, 2008, **47**, 5910–5918.
32 C. W. Hamilton, R. T. Baker, A. Staubitz and I. Manners, *Chem. Soc. Rev.*, 2009, **38**, 279–293.
33 V. Pons, R. T. Baker, N. K. Szymczak, D. J. Heldebrant, J. C. Linehan, M. H. Matus, D. J. Grant and D. A. Dixon, *Chem. Commun.*, 2008, 6597–6599.
34 D. Pun, E. Lobkovsky and P. J. Chirik, *Chem. Commun.*, 2007, 3297–3299.
35 R. J. Keaton, J. M. Blacquiere and R. T. Baker, *J. Am. Chem. Soc.*, 2007, **129**, 1844–1845.
36 P. M. Zimmerman, A. Paul and C. B. Musgrave, *Inorg. Chem.*, 2009, **48**, 5418–5433.
37 R. P. Shrestha, H. V. Diyabalanage, T. A. Semelsberger, K. C. Ott and A. K. Burrell, *Int. J. Hydrogen Energy*, 2009, **34**, 2616–2621.
38 X. Yang and M. B. Hall, *J. Am. Chem. Soc.*, 2008, **130**, 1798–1799.
39 X. Yang and M. B. Hall, *J. Organomet. Chem.*, 2009, **694**, 2831–2838.
40 M. C. Denney, V. Pons, T. J. Hebden, D. M. Heinekey and K. I. Goldberg, *J. Am. Chem. Soc.*, 2006, **128**, 12048–12049.
41 B. L. Dietrich, K. I. Goldberg, D. M. Heinekey, T. Autrey and J. C. Linehan, *Inorg. Chem.*, 2008, **47**, 8583–8585.
42 C. A. Jaska, K. Temple, A. J. Lough and I. Manners, *Chem. Commun.*, 2001, 962–963.
43 N. Blaquiere, S. Diallo-Garcia, S. I. Gorelsky, D. A. Black and K. Fagnou, *J. Am. Chem. Soc.*, 2008, **130**, 14034–14035.
44 V. Pons and R. T. Baker, *Angew. Chem., Int. Ed.*, 2008, **47**, 9600–9602.
45 S. Hausdorf, F. Baitalow, G. Wolf and F. O. Mertens, *Int. J. Hydrogen Energy*, 2008, **33**, 608–614.
46 N. C. Smythe and J. C. Gordon, *Eur. J. Inorg. Chem.*, 2010, 509–521.
47 B. L. Davis, D. Dixon, E. Garner, J. Gordon, M. Matus, B. Scott and F. Stephens, *Angew. Chem., Int. Ed.*, 2009, **48**, 6812–6816.
48 A. D. Sutton, B. L. Davis, K. X. Bhattacharyya, B. D. Ellis, J. C. Gordon and P. P. Power, *Chem. Commun.*, 2010, **46**, 148–149.
49 G. E. Ryschkewitsch, *J. Am. Chem. Soc.*, 1960, **82**, 3290–3294.
50 T. Umegaki, J.-M. Yan, X.-B. Zhang, H. Shioyama, N. Kuriyama and Q. Xu, *Int. J. Hydrogen Energy*, 2009, **34**, 3816–3822.
51 J.-M. Yan, X.-B. Zhang, S. Han, H. Shioyama and Q. Xu, *Angew. Chem., Int. Ed.*, 2008, **47**, 2287–2289.

52 X. Yang, F. Cheng, J. Liang, Z. Tao and J. Chen, *Int. J. Hydrogen Energy*, 2009, **34**, 8785–8791.
53 V. I. Simagina, P. A. Storozhenko, O. V. Netskina, O. V. Komova, G. V. Odegova, Y. V. Larichev, A. V. Ishchenko and A. M. Ozerova, *Catal. Today*, 2008, **138**, 253–259.
54 S. B. Kalidindi, M. Indirani and B. R. Jagirdar, *Inorg. Chem.*, 2008, **47**, 7424–7429.
55 S. Basu, Y. Zheng, A. Varma, W. Delgass and J. Gore, *J. Power Sources*, 2010, **195**, 1957–1963.
56 K. Eom, M. Kim, R. Kim, D. Nam and H. Kwon, *J. Power Sources*, 2010, **195**, 2830–2834.
57 K. Eom, K. Cho and H. Kwon, *Int. J. Hydrogen Energy*, 2010, **35**, 181–186.
58 N. Patel, R. Fernandes, G. Guella and A. Miotello, *Appl. Catal., B*, 2010, **95**, 137–143.
59 M. Chandra and Q. Xu, *J. Power Sources*, 2007, **168**, 135–142.
60 F. Durap, M. ZahmakIran and S. Özkar, *Int. J. Hydrogen Energy*, 2009, **34**, 7223–7230.
61 S. Basu, A. Brockman, P. Gagare, Y. Zheng, P. V. Ramachandran, W. N. Delgass and J. P. Gore, *J. Power Sources*, 2009, **188**, 238–243.
62 M. Chandra and Q. Xu, *J. Power Sources*, 2006, **156**, 190–194.
63 M. Chandra and Q. Xu, *J. Power Sources*, 2006, **159**, 855–860.
64 V. K. Srivastava, R. S. Shukla, H. C. Bajaj and R. V. Jasra, *J. Mol. Catal. A: Chem.*, 2003, **202**, 65–72.
65 B. R. James, L. D. Markham, B. C. Hui and G. L. Rempel, *J. Chem. Soc., Dalton Trans.*, 1973, 2247–2252.
66 M. E. Bluhm, M. G. Bradley, R. Butterick, U. Kusari and L. G. Sneddon, *J. Am. Chem. Soc.*, 2006, **128**, 7748–7749.
67 A. C. Stowe, W. J. Shaw, J. C. Linehan, B. Schmid and T. Autrey, *Phys. Chem. Chem. Phys.*, 2007, **9**, 1831–1836.
68 H. Benoît and P. Piejus, *C. R. Acad. Sci., Ser. B*, 1967, **265**, 101–104.
69 J. Oddershede, J. Geertsen and G. E. Scuseria, *J. Phys. Chem.*, 1988, **92**, 3056–3059.
70 P. Piejus,, *C. R. Acad. Sci., Ser. B*, 1967, **265**, 785–788.
71 T. Schwabe and S. Grimme, *Acc. Chem. Res.*, 2008, **41**, 569–579.
72 K. Müller-Dethlefs and P. Hobza, *Chem. Rev.*, 2000, **100**, 143–167.
73 D. Hugas, S. Simon, M. Duran, C. Fonseca-Guerra and F. M. Bickelhaupt, *Chem.–Eur. J.*, 2009, **15**, 5814–5822.
74 S. R. Gadre, S. A. Kulkarni and I. H. Shrivastava, *J. Chem. Phys.*, 1992, **96**, 5253–5260.
75 P. Dani, T. Karlen, R. A. Gossage, W. J. J. Smeets, A. L. Spek and G. van Koten, *J. Am. Chem. Soc.*, 1997, **119**, 11317–11318.
76 E. C. Constable, S. J. Dunne, D. G. F. Rees and C. X. Schmitt, *Chem. Commun.*, 1996, 1169–1170.
77 A. Toner, J. Matthes, S. Gründemann, H. H. Limbach, B. Chaudret, E. Clot and S. Sabo-Etienne, *Proc. Natl. Acad. Sci. U. S. A.*, 2007, **104**, 6945–6950.
78 G. Alcaraz, M. Grellier and S. Sabo-Etienne, *Acc. Chem. Res.*, 2009, **42**, 1640–1649.
79 M. Shimoi, S. Nagai, M. Ichikawa, Y. Kawano, K. Katoh, M. Uruichi and H. Ogino, *J. Am. Chem. Soc.*, 1999, **121**, 11704–11712.
80 T. J. Marks and J. R. Kolb, *Chem. Rev.*, 1977, **77**, 263–293.
81 G. Alcaraz and S. Sabo-Etienne, *Coord. Chem. Rev.*, 2008, **252**, 2395–2409.
82 R. N. Perutz and S. Sabo-Etienne, *Angew. Chem., Int. Ed.*, 2007, **46**, 2578–2592.